

Article

Microstructure and Mechanical Property of Mg-3Al-1Zn Magnesium Alloy Sheet Processed by Integrated High Temperature Rolling and Continuous Bending

Yong Lian ¹, Benhong Liao ², Tao Zhou ^{2,*}, Wenjun Ge ², Laixin Shi ^{2,*}, Li Hu ²,
Mingbo Yang ² and Jin Zhang ¹

¹ Institute for Advanced Materials and Technology, University of Science and Technology Beijing, Beijing 100083, China; liany09@126.com (Y.L.); zhangjin@ustb.edu.cn (J.Z.)

² College of Material Science and Engineering, Chongqing University of Technology, Chongqing 400054, China; liaobenhong@2017.cqut.edu.cn (B.L.); gwj53231323@2017.cqut.edu.cn (W.G.); huli@cqut.edu.cn (L.H.); yangmingbo@cqut.edu.cn (M.Y.)

* Correspondence: zt19811118@cqut.edu.cn (T.Z.); shilaixin2016@cqut.edu.cn (L.S.);
Tel.: +86-186-9669-8252 (T.Z.); +86-151-2337-6156 (L.S.)

Received: 14 February 2020; Accepted: 12 March 2020; Published: 16 March 2020



Abstract: In the present study, we developed an integrated process that combined high-temperature rolling and continuous bending as a single processing step, i.e., the HTR-CB process, and the process was carried out on Mg-3Al-1Zn magnesium alloy sheet in order to improve its ductility at room temperature. The microstructure, texture and mechanical property of the HTR-CB sample were investigated. The results show that the HTR-CB sample after annealing exhibits a high Erichsen value of 6.9, which is more than 1.5 times larger than that (4.6) in the HTR sheet, mainly due to the formation of non-basal textures with double peaks titling at the range of $\pm 30^\circ \sim \pm 38^\circ$ from the normal direction towards the rolling direction. The main reasons for the texture modifications during the HTR-CB process and annealing are discussed.

Keywords: magnesium alloy; high-temperature rolling; continuous bending; texture; mechanical property

1. Introduction

Due to their low density and high specific strength, the interest in magnesium (Mg) alloys has increased in recent years for weight-critical applications in aerospace, automobile and electronic industries [1,2]. However, the poor ductility and sheet formability at ambient temperatures due to the hexagonal close-packed structure of Mg alloys presents a serious problem [3,4]. Additionally, wrought Mg alloy sheet processed by conventional plastic deformation methods such as extrusion and rolling exhibits a strong basal texture, which will give rise to deteriorating the sheet formability. It has been reported that the ductility of the Mg alloy sheets at room temperature can be improved by means of texture control through severe plastic deformation (SPD), such as equal channel angular extrusion (ECAE) [5–8]. However, the ECAE process is not suitable to fabricate wide Mg alloy sheets [9]. Recently, Huang et al. [10] have found that by increasing the rolling temperature up to 525 °C, the Erichsen value of AZ31 alloy sheets can be improved up to 8.6, due to the remarkable basal texture weakening after annealing. Additionally, they suggested that the rotation of nuclei and small static recrystallization (SRX) grains in various directions during annealing may be promoted by the absorption of non-basal dislocations in boundaries, which leads to the remarkable weakened basal texture [11]. Thus, HTR is beneficial to the improvement of the sheet formability at ambient temperatures. In addition, it has been reported that for the AZ31 alloy sheets processed by repeated unidirectional bending (RUB) at room

temperature, the c-axis tends to incline toward the RD, which leads to the Erichsen value and limiting drawing ratio reaching 5.9 and 1.5mm at room temperature, respectively [12,13]. Huang et al. [14] have studied the microstructures, textures and properties of AZ31Mg alloy sheets processed by RUB ranging from 200 to 400 °C, and found that the texture components become more disperse with increasing the RUB temperatures. For the AZ31 alloy sheet processed by bidirectional cyclic bending (BCB) at 150 °C, after annealing, the fine grains and weakened basal texture in the regions near the two surfaces can be obtained, and the total elongation ranges up to 37.7% [15]. However, the studies related to the multi-pass continuous bending (CB) are always focused on the microstructures and properties of Mg alloy sheets processed by RUB or BCB at lower and medium temperatures, so the relationship between the multi-pass CB at high temperature and the microstructure, texture and stretch formability of the Mg alloy sheets is unclear. Therefore, in the present study, we developed an integrated process that combined HTR and CB in a single processing step, i.e., the HTR-CB process, and the HTR-CB process was carried out on AZ31 magnesium alloy sheet. The evolutions of microstructure, texture and mechanical property of the sheets were investigated.

2. Experimental Procedure

The initial material used in the study was an AZ31 alloy (Mg-3Al-1Zn-0.3Mn, in wt %) sheet with a width of 120 mm and thickness of 1.26 mm prepared by symmetric hot rolling with 6 passes from 4.3 mm in thickness. The sheet was pre-heated at 550 °C for 1 min, and then rolled at a thickness reduction of 5% into the HTR-CB device, as shown in Figure 1. The channel height (H) was a constant value of 2.0 mm. The oblique angles (θ) of all corners were 120° and the distance (K) between the axes of two parallel channels was 11 mm [16]. For corner 1 of the mold, the internal radius (r) and the external radius (R) were 3 mm and 0 mm, respectively, and for following three corners, both r and R were 10 mm [16]. It can be seen that except for the channel height, the design and the other parameters of the HTR-CB mold was the same as that of the equal channel angular rolling-continuous bending mold (ECAR-CB) [17], because the main difference between the HTR and ECAR-CB process was that the main deformation mode at corner 1 of the mold was shear or bend deformation. It means that for the ECAR-CB process the sheet underwent shear deformation at corner 1 and bend deformation at the corner 2, 3 and 4, however, for the HTR-CB process the sheet underwent bend deformation at the corner 1, 2, 3 and 4. It was reported that with an increase in internal radius (r) of the ECAR die, the shear strain and angle at one pass were decreased and the main deformation mode was translated from shear deformation to bend deformation gradually [18]. Moreover, Cheng et al. [19] found that the shear strain decreased with an increase in the channel clearance (c) of the ECAR mold, which was defined as a ratio of channel height (H) to sheet thickness (t), i.e. $c = H/t$. Thus, it can be concluded that the main deformation mode (shear or bend deformation) at the corner of ECAR mold was controlled by the value of r [18,20] and c [19]. For the present study, the r and θ of all corners of the HTR-CB mold was the same as that of the ECAR-CB mold. Thus, the channel clearance of the mold will dominate the main deformation mode. According to Ref. [19], when the c was 1.29, the shear angle was about only 4°, so the shear deformation does almost not occur during the ECAR process [19]. Thus, in the present study, the channel height (H = 2.0 mm), i.e., $c = 1.67$, which was much higher than 1.29, can achieve the bend deformation at corner 1 of the mold. Before HTR-CB process, the mold was lubricated by graphite and the mold was not heated. The HTR-CB deformation was performed at one pass. The radius of the rollers was 175 mm and the rolling speed was 0.4 m/s. For comparison, the as-received sheet was obtained by symmetrical rolling at 550 °C from 1.26 mm to 1.2 mm in thickness by one pass. After rolling, the as-received sheets and HTR-CBed sheets were annealed at 300 °C for 1h to carry out the tensile and Erichsen tests at room temperature. For simplicity, the as-received sample, the HTR-CB sample and the subsequently corresponding annealed samples can be defined as HTR sample, HTR-CB sample (Figure 1b), HTRA sample and HTR-CBA sample, respectively.

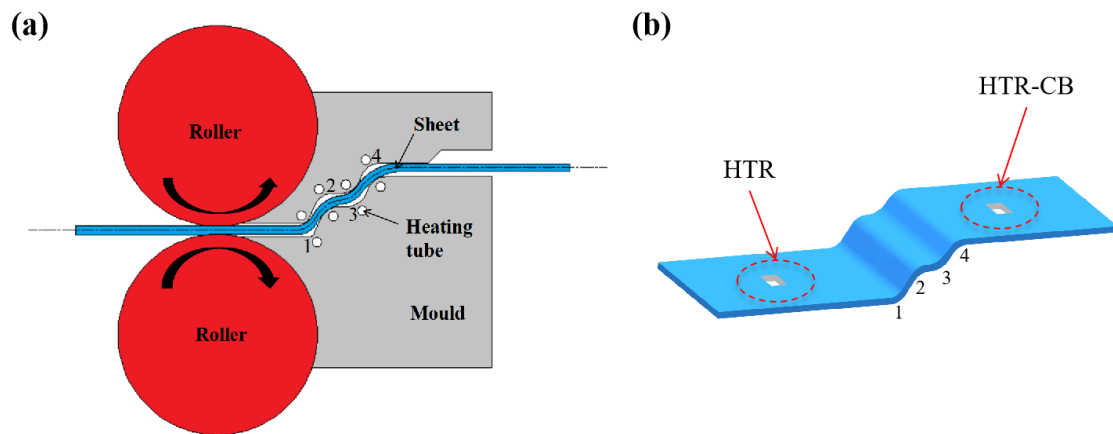


Figure 1. (a) Schematic illustration of the high-temperature rolling and continuous bending (HTR-CB) process (bend deformation in corner 1, 2, 3 and 4); (b) Schematic illustration of the HTR and HTR-CB samples.

The microstructure and texture evolution were revealed by electron back-scatter diffraction (EBSD), which was conducted on a FEI NOVA 400 scanning electron microscope (FEI Corporation, Hillsboro, OR, USA) equipped with a HKL-EBSD system using a step size of 0.5 μm . The tensile tests were carried out at the angle of 0° (RD) to the rolling direction on a SANS testing machine with an initial strain rate of $10^{-3}/\text{s}$ at room temperature. The specimens for tensile tests had a gauge length of 15 mm, a width of 4 mm and a thickness of 1.2 mm. The Lankford values (*r*-value), $r = \varepsilon_w/\varepsilon_t$, where the ε_w and ε_t were the strains along the plate width and thickness directions, respectively, were measured on the samples at a nominal deformation of $\varepsilon = 12\%$. Moreover, circular blanks with a diameter of 60 mm were machined from the sheets for Erichsen tests without lubrication. The Erichsen tests were carried out using a semi-spherical punch having a diameter of 20 mm. The punch speed was about 4 mm/min and the blank holder force was 10 kN. The average Erichsen values (AVE IE) were given by averaging the IE from two Erichsen tests for each sheet.

3. Results and Discussion

3.1. Microstructures Evolution

Figure 2 shows the EBSD inverse pole figure (IPF) maps, boundary misorientation maps, kernel average misorientation (KAM) maps and misorientation angle distributions of the HTR and HTR-CB samples. It can be seen that both the upper surface and mid-layer of the HTR sample (Figure 2a₁, b₁) exhibit equiaxed grains, and some of which are occupied with a few (10–12) extension twins (Figure 2a₂, b₂). The average grain size of the upper surface and mid-layer are about 23 and 26 μm , respectively. The grain orientations of the two HTR samples are similar, which are mainly in red color, indicating that the upper surface and mid-layer both exhibit a strong basal texture. Moreover, a peak at $\sim 3^\circ$ is observed in the misorientation angle distribution images of the two HTR samples (Figure 2a₄, b₄), which means that a high fraction of low angle grain boundaries (LAGBs) can be introduced by symmetrical rolling at 550 $^\circ\text{C}$. It indicates that HTR sample contains a mass of dislocations. This issue can be further enhanced by the KAM maps of the HTR samples, as seen in Figure 2a₃, b₃. After HTR-CB, however, a large number of {10–12} extension twins are introduced both in the upper surface and mid-layer, as seen in Figure 2c₁, c₂, d₁, d₂. The phenomenon can be confirmed by Figure 2c₄, d₄, where peaks at $\sim 90^\circ$ are observed in the misorientation angle distribution images. It has been reported that the convex surface of the sheet suffered tension stress while the concave surface suffered compression stress during bending [15]. Hong et al. have suggested that (10–12) twinning can only be activated through a compressive stress perpendicular to the *c*-axis of grain or a tensile stress parallel to the *c*-axis of grain [21]. Therefore, for the as-rolled sheet with a strong basal texture,

(10–12) twinning only can be activated in the concave surface. So, it seems that a lot of (10–12) twins occur in the mid-layer of the HTR-CB sheet in the present study is puzzling. It should be noted that the stress state of the sheet during the HTR-CB process is special, i.e., as the sheet is compressed into the bending mold as shown in Figure 1, it will be subjected to a compression stress along the RD at the corner of the mold, which is beneficial to the activation and growth of (10–12) twins with c-axis//RD. Similar with the HTR sample, the HTR-CB samples also contains a mass of dislocations, as seen in Figure 2c₃,d₃,c₄,d₄. Figure 3 illustrate the number fraction of matrix grains with c-axis//ND and {10-12} twins in different states. In the figure, the HTR-s and HTR-CB-s are for upper surface of HTR and HTR-CB samples, and the HTR-m and HTR-CB-m are for mid-layer of HTR and HTR-CB samples, respectively. It can be seen that compared with the HTR samples, after the HTR-CB, the number of the matrix grains dramatically decreases but the (10–12) twins increase, which suggests that the matrix grains are gradually consumed by (10–12) twins during the HTR-CB process. In addition, for the HTR-CB sample, the volume fraction of the (10–12) extension twins in the upper surface is higher than that in mid-layer, which may be due to that the strain accumulated near the surfaces is higher than that in the mid-layer of the sheet during the bending [15]. This phenomenon is different with the results in ECAR-CB [16].

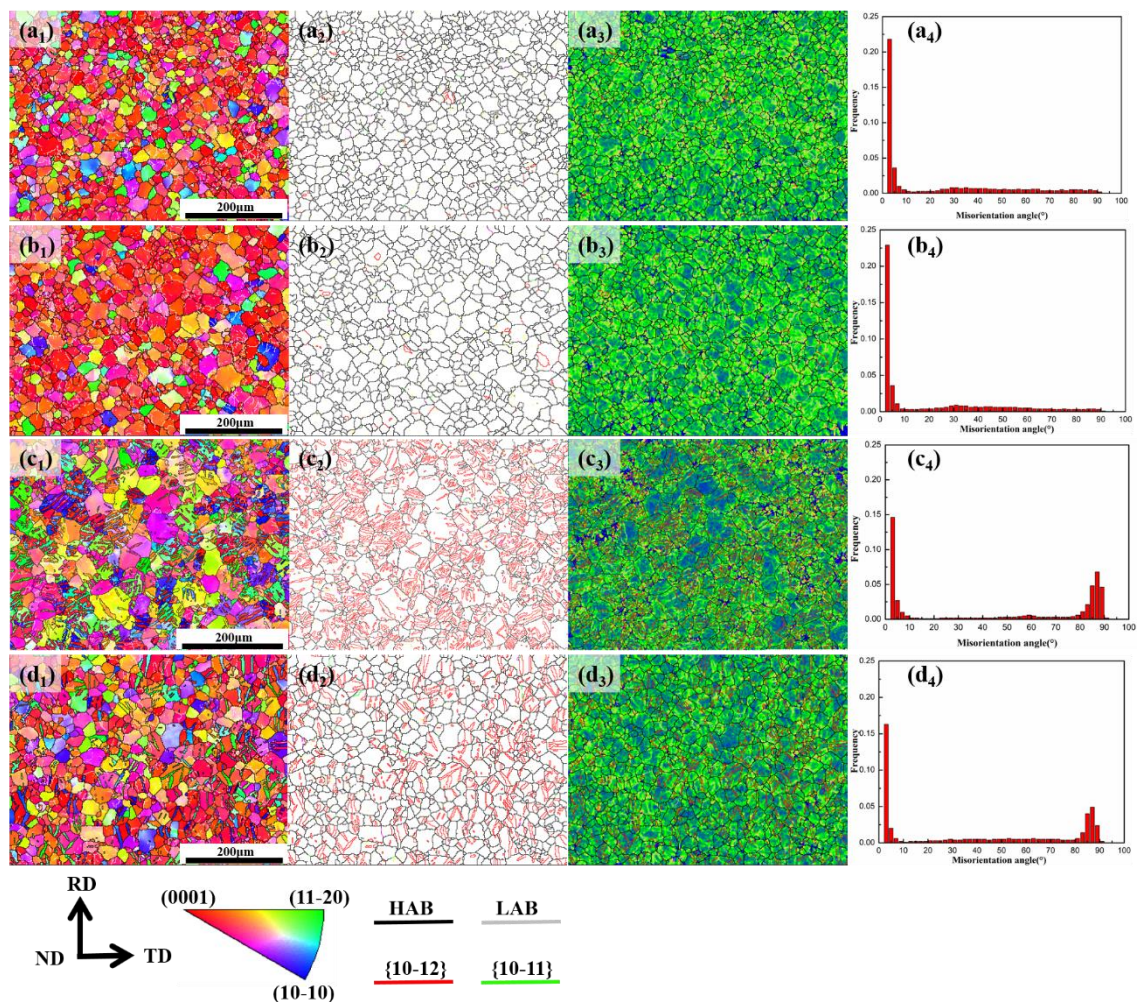


Figure 2. Electron back-scatter diffraction (EBSD) results from the different samples without annealing: (a) upper surface of HTR sample; (b) mid-layer of HTR sample; (c) upper surface of HTR-CB sample; (d) mid-layer of HTR-CB sample, including inverse pole figure maps, boundary misorientation maps, kernel average misorientation maps and misorientation angle distributions.

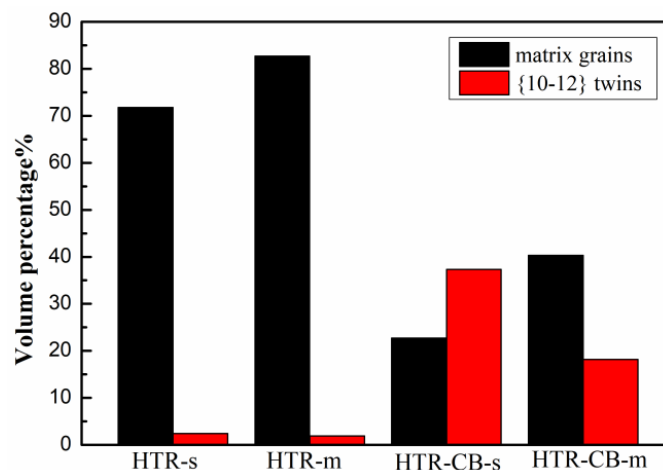


Figure 3. The number fraction of matrix grains with c -axis//ND and $\{10\text{--}12\}$ twins in different states, and the HTR-s and HTR-CB-s are for upper surface of HTR and HTR-CB samples, and the HTR-m and HTR-CB-m are for mid-layer of HTR and HTR-CB samples, respectively

Figure 4 demonstrates the EBSD inverse pole figure (IPF) maps, boundary misorientation maps and misorientation angle distributions of the HTRA and HTR-CBA samples. It can be seen that after annealing, the $\{10\text{--}12\}$ twins almost disappear and the upper surface and mid-layer of the all the samples exhibit static recrystallized grain structures. As seen in Figure 5, the average grain size near upper surface and mid-layer of the HTRA sample is approximately $17\ \mu\text{m}$ and $18\ \mu\text{m}$, respectively. For the HTR-CBA sample, the average grain size near the upper surface and mid-layer is $14\ \mu\text{m}$ and $15\ \mu\text{m}$, respectively, a little smaller than that of HTRA sample. Moreover, for the HTR-CB sheet underwent annealing, the grain size near the upper surface is similar with that in the mid-layer, which is different with the results in BCB AZ31 alloy sheet [22]. It has been reported that after BCB and annealing, the remarkably gradient structure is observed, i.e., until fine grains are near the surfaces and coarse grains are in the mid-layer [22], which is mainly due to the fact that the sheet underwent BCB, and the plastic strain is mostly focused near the upper and lower surfaces, but the strain in the central is very small, which leads to that the driving force of SRX near the surfaces is much higher than that in the central during the subsequent annealing. However, as mentioned above, the sheet can be subjected to a compression stress along the RD during HTR-CB process, which leads to that a lot of twins can be produced in the mid layer of the sheet (Figure 2d₁,d₂). Meanwhile, a mass of dislocations are also observed in the mid layer (Figure 2d₃,d₄). The deformation stored energy in the mid layer of the HTR-CB sheet may be high enough for the SRX during the subsequent annealing. Thus, the gradient structure along the thickness is not significant for the sheet that underwent HTR-CB and annealing.

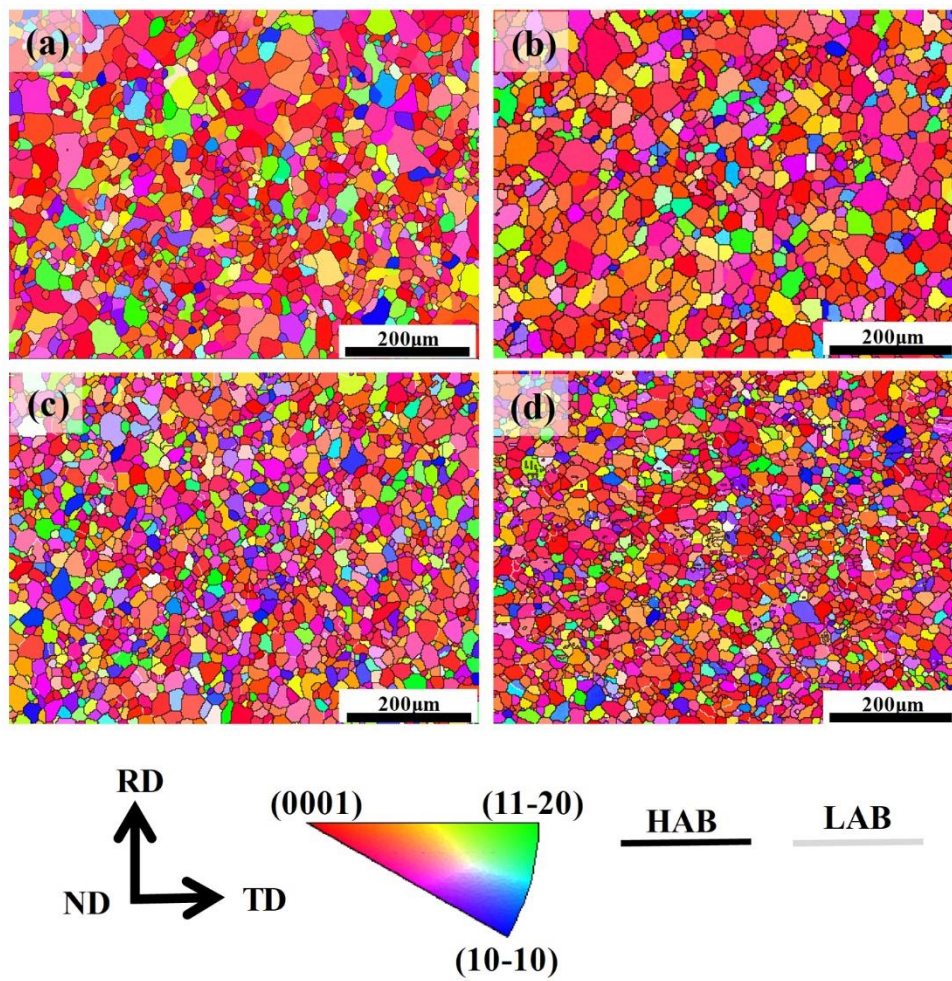


Figure 4. Inverse pole figure maps of different samples after annealing: (a) upper surface of HTRA sample; (b) mid-layer of HTRA sample; (c) upper surface of HTR-CBA sample; (d) mid-layer of HTR-CBA sample.

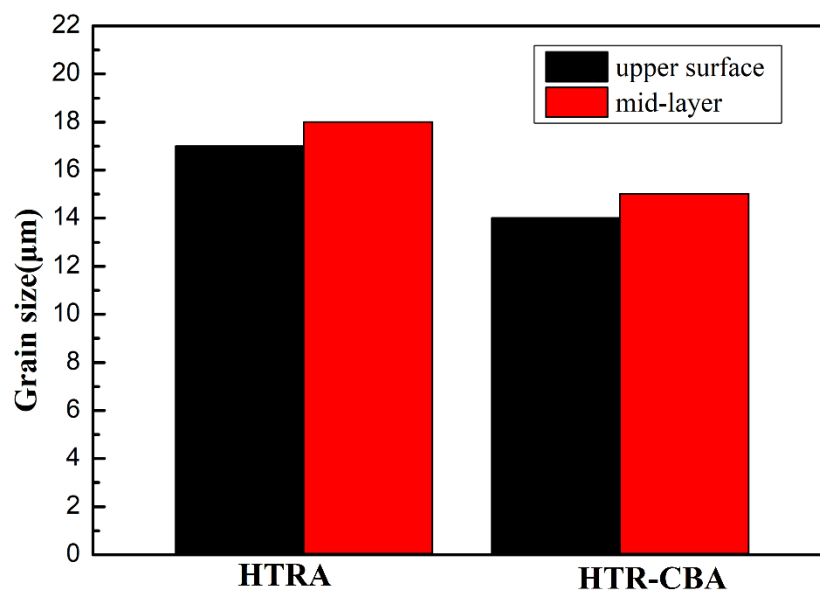


Figure 5. The average grain size of HTRA and HTR-CBA samples.

3.2. Texture Evolution

The (0002) pole figures of the sheets underwent HTR-CB without annealing are shown in Figure 6. In the as-rolled condition, both of the upper surface (Figure 6a) and mid-layer (Figure 6b) of the HTR sheet display a strong basal texture and the basal poles incline at 10° toward the RD, which is mainly due to the activation of the $\langle c+a \rangle$ slip during rolling [23]. After HTR-CB (Figure 6c,d), the c -axis of most grains of the upper surface and mid-layer rotates approximately 90° away from ND toward RD, resulted from the occurrence of (10–12) tension twinning, as seen in Figures 2 and 3. So compared with the upper surface and mid-layer of HTR sheet with the basal texture intensity of 8 and 8.5, the remarkably weakened basal texture intensity of 2.1 and 5.8 can be obtained for the HTR-CB sheet, respectively, and the major texture component dramatically changed from the center of the (0002) pole figure to the RD, which means that the (10–10) prismatic texture component with c -axis//RD preferred orientation is enhanced. In addition, the basal poles of these twins lie within about $\pm 30^\circ$ from the RD to TD (Figure 6c,d). This phenomenon is similar with the results when the AZ31 alloy magnesium alloy sheet is employed by in-plane precompression along the RD [24] or ED [25], which is due to that only one pair of the potential twin variants whose c -axis adjacent to the loading axis can be activated under the compression condition, because of the strict SF law of the twinning behavior [25,26]. Thus, it can be inferred that the special stress state of the sheet during the HTR-CB process, i.e., a compression stress along the RD at the corner of the HTR-CB mold may be the main reason for the selection of the basal poles of the (10–12) tension twins.

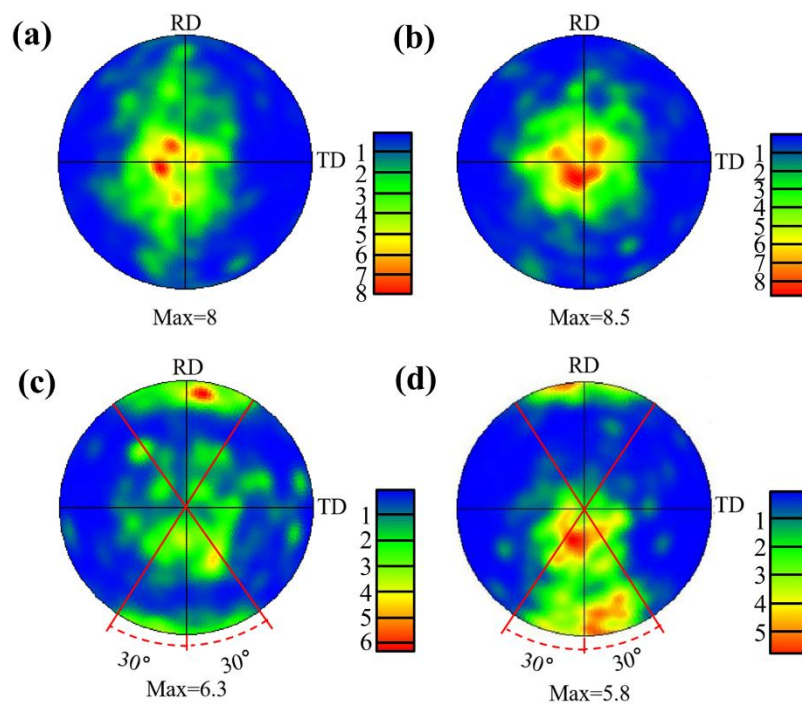


Figure 6. (0002) Pole figures of the different samples without annealing: (a) upper surface of HTR sample; (b) mid-layer of HTR sample; (c) upper surface of HTR-CB sample; (d) mid-layer of HTR-CB sample.

After annealing, both of the upper surface (Figure 7a) and mid-layer (Figure 7b) of the HTR samples still exhibited a typical basal texture with basal poles tilting at approximately $\pm 10^\circ$ in the RD, similar with that of HTR samples. However, for the HTR-CBA samples (Figure 7c,d), the (10–10) prismatic texture components in (0002) pole figure disappeared, due to the (10–12) tensile twins disappeared during the SRX. Moreover, the upper surface (Figure 7c) and mid-layer (Figure 7d) of the HTR-CBA samples exhibit double-peak texture with the basal poles tilting at approximately $\pm 38^\circ$ and $\pm 30^\circ$ in the RD, respectively, which are smaller than that of ECAR-CBA [16]. It should be noted that the two basal poles are completely split (Figure 7c,d), so the texture characteristics of the HTR-CBA

sample is non-basal texture, which is different with that by RUB [16], BCB [22], high-temperature rolling [27]. Jiang et al. [28,29] have reported that after small strain impact multi-directional forging (SSIMDF) 200 passes for AZ61 Mg alloy, a very weakened double-peak texture with two basal poles completely split are obtained, mainly attributes to the twinning and DRX during SSIMDF. Zhu et al. [30] have found that for the ZK60 Mg alloy samples rolled at high strain rates, the peak intensity regions deviates from the center of the (0002) pole figure by large angles and the peaks tends to completely split, which mainly due to the (10–11)-(10–12) double twinning and completely DRX. However, in the present work the non-basal texture is obtained during SRX, rather than DRX, so the reason may be different. Huang et al. [11] have suggested that the rotation of nuclei and small SRX grains in various directions during annealing may be promoted by the absorption of non-basal dislocations in boundaries, which leads to a remarkable weakened texture. Increasing the deformation temperature enhances the activities of grain boundary slip (GBS), which may affect the SRX kinetics [10]. In addition, Sanjari et al. [31] have suggested that during annealing, the compressive twins, second twins and their vicinity may be the preferred sites for nucleation, which is beneficial to the basal texture weakening. For the HTR-CB samples, the high rolling temperature of 550 °C is carried out, which is beneficial to the activation of the $\langle c+a \rangle$ dislocations and GBS. Meanwhile, the area fractions of tensile twins in HTR-CB sheet are increased compared with that in HTR sheet (Table 1). Therefore, it can be inferred that the formation of the non-basal texture may be mainly related to the influence of $\langle c+a \rangle$ dislocations and twins on the SRX behavior. The detailed mechanism needs to be further studied.

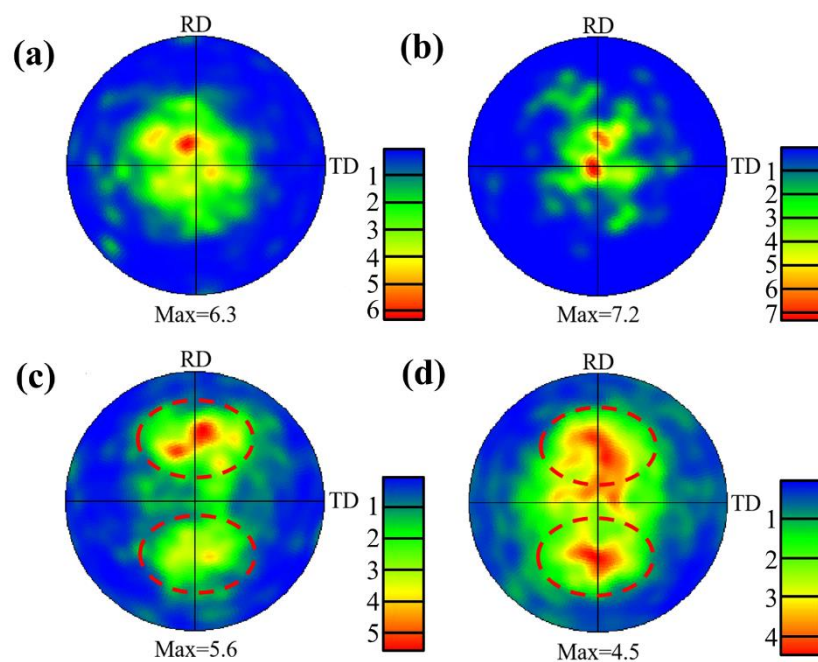


Figure 7. (0002) Pole figures of the different samples after annealing: (a) upper surface of HTRA sample; (b) mid-layer of HTRA sample; (c) upper surface of HTR-CBA sample; (d) mid-layer of HTR-CBA sample.

3.3. Mechanical Properties

The flow curves obtained from the tensile test along the RD are displayed in Figure 8. The corresponding detailed mechanical properties, including the 0.2% proof yield stress (YS), the ultimate tensile strength (UTS), the fracture elongation (FE), the ratio of YS and UTS (YS/UTS), the strain hardening exponent (n) and the Lankford value (r-value) are listed in Table 1. Compared with the HTRA sample, the HTR-CBA sample exhibit the much lower YS, slightly larger FE, smaller r-value and larger n-value. It is well known that the YS, r-value and n-value of the Mg sheets is strongly influenced by the grain size [32] and texture [33]. However, in the present study, the HTRA

and HTR-CBA samples have the similar grain size, so the difference in mechanical properties can be mainly attributed to the texture modification by the HTR-CB. According to the previous study [31], the weakened texture leads to the Schmid factor of basal $\langle a \rangle$ slip increasing, beneficial to the decrease in the YS. For grains with the tilt basal texture, the thickness strain can be accommodated by basal slip, prismatic slip and extension twinning [33]. Thus, the r -value can be effectively decreased by the weakened basal texture. Meanwhile, with the weakened basal texture, the softening behavior of dynamic recovery resulted from the cross-slip of $\langle a \rangle$ dislocations from basal to prismatic planes can be restricted [33] and the (10–12) twinning can be activated [31], which leads to the increase in the n -value. As seen in Figure 7, the non-basal textures with double peaks titling at the range of $\pm 30^\circ \sim \pm 38^\circ$ from the ND towards the RD can be formed in the HTR-CBA sample, thus, the lower YS, smaller r -value and larger n -value are obtained in the HTR-CBA sample.

Figure 9 presents the average values (AVE) of IE of the sheets with the semi-spherical deformations by the Erichsen test. It can be seen that the AVE IE of the HTRA sample is 4.6, but the HTR-CBA sample exhibits a much higher IE of 6.9, which is higher than that (5.9) of RUBed sheet [12], lower than that (7.4) of ECAR-CBA sheet [16]. Compared with HTRA sample, the stretched formability of the HTR-CBA sample is remarkably enhanced more than 1.5 times. It is well known that the larger n -value is, the more enhanced local strain ability of the sheet during forming and the more uniform strain distribution can be obtained, resulted in the improved forming limit. The stress state is the biaxial tension for the stretch forming, which means that the thickness strain is necessary during the biaxial tension [10]. So, the smaller r -value is beneficial to the enhanced thickness thinning of the sheet during the stretch forming, leads to the improvement of the stretch formability. In addition, the low YS is beneficial to reduce the spring back of Mg alloy sheets after shape forming [34]. Therefore, the remarkable enhanced stretch formability of the AZ31 alloy sheet processed by HTR-CB and subsequent annealing is mainly resulted from the lower YS and larger n -value, due to the formation of non-basal texture.

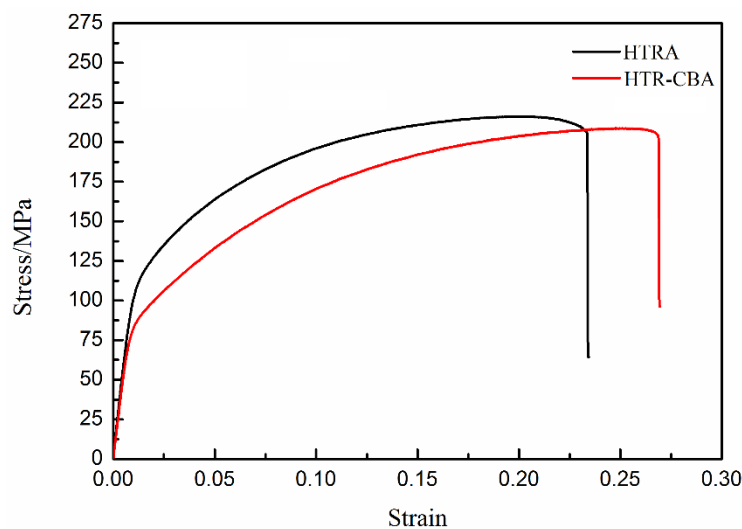


Figure 8. The stress-strain curves of the HTRA and HTR-CBA samples along the RD.

Table 1. Mechanical properties of the HTRA and HTR-CBA samples along the RD.

Samples	YS (MPa)	UTS (MPa)	FE(%)	YS/UTS	n-Value	r-Value
HTRA	105	216	23.57	0.49	0.35	1.28
HTR-CBA	82	209	27.37	0.39	0.42	0.53

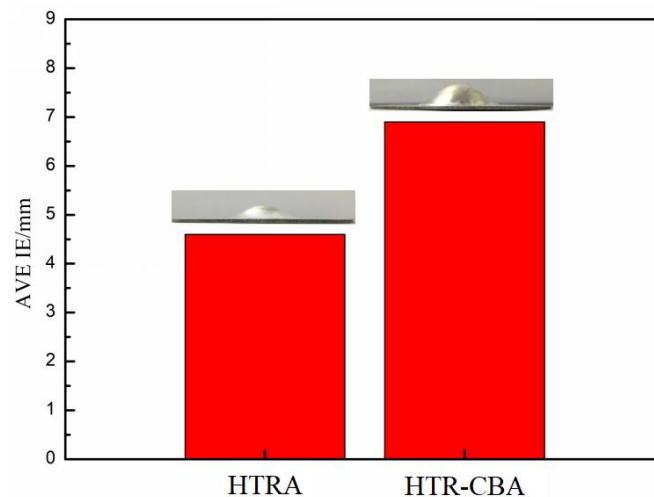


Figure 9. Room temperature formability of the HTRA and HTR-CBA samples.

4. Conclusions

In the present study, we developed an integrated process that combined high-temperature rolling and continuous bending in a single processing step, i.e. HTR-CB process, and the HTR-CB process was carried out on AZ31 magnesium alloy sheet. The microstructure, texture, mechanical property and stretch formability of the sheets were investigated. The main results are as follows:

(1) In as-rolled condition, compared with HTR sample, the HTR-CB sample exhibits the increased volume fraction of the twins but weakened basal texture intensity. Moreover, the major texture component for the HTR-CB sample dramatically changes from the center of the (0002) pole figure to the RD, which mainly due to the (10–12) tension twinning

(2) After annealing, the HTRA sample still exhibits a typical basal texture with basal poles tilting at approximately $\pm 10^\circ$ in the RD. However, for the annealed HTR-CBA sample, the non-basal textures with double peaks titling at the range of $\pm 30^\circ \sim \pm 38^\circ$ from the normal direction towards the rolling direction are obtained, in which the two basal poles are completely split, which may be mainly related to the influence of $\langle c+a \rangle$ dislocations and twins on the SRX behavior.

(3) The HTR-CB sheet followed by annealing exhibits a high Erichsen value of 6.9 at room temperature, which is more than 1.5 times larger than that (4.6) in the HTR sheet, mainly resulted from the formation of non-basal texture. Thus, HTR-CB process can be an efficient way to enhance the stretch formability of AZ31 alloy sheet at room temperature, which is beneficial to expand the application of wrought magnesium alloy sheet.

Author Contributions: Conceptualization, methodology, visualization and writing—original draft preparation, Y.L.; data curation and software, B.L., W.G.; validation and writing—review and editing, T.Z., L.S.; formal analysis, L.H.; supervision, M.Y. and J.Z. All authors have read and agree to the published version of the manuscript.

Funding: The work was financially supported by the National Key Research and Development Program of China (No. 2016YFB0301105), the National Natural Science Foundation of China (Grant Nos. 51701034, 51805064, 51501026), the Basic and Advanced Research Project of CQ CSTC (Grant Nos. cstc2016jcyjA0452, cstc2017jcyjAX0062, cstc2018jcyjAX0035).

Conflicts of Interest: The authors declare no conflict of interest.

References

1. Dogan, E.; Vaughan, M.W.; Wang, S.J.; Karaman, I.; Proust, G. Role of starting texture and deformation modes on low-temperature shear formability and shear localization of Mg–3Al–1Zn alloy. *Acta Mater.* **2015**, *89*, 408–422. [[CrossRef](#)]
2. Chen, Q.; Xia, X.; Yuan, B.; Shu, D.; Zhao, Z.; Han, J. Hot workfability behavior of as-cast Mg–Zn–Y–Zr alloy. *Mater. Sci. Eng. A* **2014**, *593*, 38–47. [[CrossRef](#)]

3. Huang, X.; Suzuki, K.; Chino, Y.; Mabuchi, M. Influence of aluminum content on the texture and sheet formability of AM series magnesium alloys. *Mater. Sci. Eng. A* **2015**, *633*, 144–153. [[CrossRef](#)]
4. Chen, Q.; Yuan, B.G.; Zhao, G.Z.; Shu, D.Y.; Hu, C.; Zhao, Z.; Zhao, Z. Microstructural evolution during reheating and tensile mechanical properties of thixoforged AZ91D-RE magnesium alloy prepared by squeeze casting–solid extrusion. *Mater. Sci. Eng. A* **2012**, *537*, 25–38. [[CrossRef](#)]
5. Sabirov, I.; Perez-Prado, M.T.; Molina-Aldareguia, J.M.; Semenova, I.P.; Salimgareeva, G.K.; Valiev, R.Z. Anisotropy of mechanical properties in high-strength ultra-fine-grained pure Ti processed via a complex severe plastic deformation route. *Scripta Mater.* **2011**, *64*, 69–72. [[CrossRef](#)]
6. Chen, Q.; Zhao, Z.X.; Shu, D.Y.; Zhao, Z.D. Microstructure and mechanical properties of AZ91D magnesium alloy prepared by compound extrusion. *Mater. Sci. Eng. A* **2011**, *528*, 3930–3934. [[CrossRef](#)]
7. Zhao, Z.D.; Chen, Q.; Chao, H.Y.; Hu, C.K.; Huang, S.H. Influence of equal channel angular extrusion processing parameters on the microstructure and mechanical properties of Mg–Al–Y–Zn alloy. *Mater. Des.* **2011**, *32*, 575–583. [[CrossRef](#)]
8. Kim, W.J.; Hong, S.I.; Kim, Y.S.; Min, S.H.; Jeong, H.T.; Lee, J.D. Texture development and its effect on mechanical properties of an AZ61 Mg alloy fabricated by equal channel angular pressing. *Acta Mater.* **2003**, *51*, 3293–3307. [[CrossRef](#)]
9. Li, X.; Jiang, B.; He, J.J.; Zhang, J.Y.; Jiang, Z.T.; Liu, B.; Pan, F.S. Improvement of planar isotropy, mechanical properties and corrosion resistance of extruded Mg–3Al–1Zn alloy sheet by special grain re-orientation. *J. Alloys Compd.* **2017**, *721*, 106–117. [[CrossRef](#)]
10. Huang, X.S.; Suzuki, K.; Chino, Y.; Mabuchi, M. Improvement of stretch formability of Mg–3Al–1Zn alloy sheet by high temperature rolling at finishing pass. *J. Alloys Compd.* **2011**, *509*, 7579–7584. [[CrossRef](#)]
11. Huang, X.S.; Suzuki, K.; Chino, Y.; Mabuchi, M. Influence of rolling temperature on static recrystallization behavior of AZ31 magnesium alloy. *J. Mater. Sci.* **2012**, *47*, 4561–4567. [[CrossRef](#)]
12. Zhang, L.; Huang, G.S.; Zhang, H.; Song, B. Cold stamping formability of AZ31B magnesium alloy sheet undergoing repeated unidirectional bending process. *J. Mater. Process. Tech.* **2011**, *211*, 644–649. [[CrossRef](#)]
13. Song, B.; Huang, G.S.; Li, H.C.; Zhang, L.; Huang, G.J.; Pan, F.S. Texture evolution and mechanical properties of AZ31B magnesium alloy sheets processed by repeated unidirectional bending. *J. Alloys Compd.* **2010**, *489*, 75–81. [[CrossRef](#)]
14. Huang, G.S.; Song, B.; Xu, W.; Zhang, L. Structure and properties of AZ31B magnesium alloy sheets processed by repeatedly unidirectional bending at different temperatures. *Trans. Nonferrous Met. Soc. China* **2010**, *20*, 1815–1821. [[CrossRef](#)]
15. Zhang, L.; Yang, X.Y.; Huo, Q.H.; Tian, F.; Zhang, Y.J.; Zhou, X.J.; Chen, J. Structure evolution of AZ31 Mg alloy sheet during bidirectional cyclic bending at low temperature and subsequent annealing. *Acta Metall. Sin.* **2011**, *47*, 990–996.
16. Song, D.H.; Zhou, T.; Tu, J.; Shi, L.X.; Song, B.; Hu, L.; Yang, M.; Chen, Q.; Lu, L. Improved stretch formability of AZ31 sheet via texture control by introducing a continuous bending channel into equal channel angular rolling. *J. Mater. Process. Tech.* **2018**, *259*, 380–386. [[CrossRef](#)]
17. Tu, J.; Zhou, T.; Liu, L.; Shi, L.X.; Hu, L.; Song, D.; Song, B.; Yang, M.; Chen, Q.; Pan, F. Effect of rolling speeds on texture modification and mechanical properties of the AZ31 sheet by a combination of equal channel angular rolling and continuous bending at high temperature. *J. Alloys Compd.* **2018**, *768*, 598–607. [[CrossRef](#)]
18. Cheng, Y.Q.; Chen, Z.H.; Xia, W.J.; Zhou, T. Deformation law of equal channel angular rolling for AZ31 magnesium alloy sheets. *J. Plast. Eng.* **2007**, *14*, 127–132.
19. Cheng, Y.Q.; Chen, Z.H.; Xia, W.J.; Zhou, T. Effect of channel clearance on crystal orientation development in AZ31 magnesium alloy sheet produced by equal channel angular rolling. *J. Mater. Process. Tech.* **2007**, *184*, 97–101. [[CrossRef](#)]
20. Luis Pérez, C.J. On the correct selection of the channel die in ECAP processes. *Scripta Mater.* **2004**, *50*, 387–393. [[CrossRef](#)]
21. Hong, S.G.; Park, S.H.; Lee, C.S. Role of {10-12} twinning characteristics in the deformation behavior of a polycrystalline magnesium alloy. *Acta Mater.* **2010**, *58*, 5873–5885. [[CrossRef](#)]
22. Huo, Q.H.; Yang, X.Y.; Ma, J.J.; Sun, H.; Wang, J.; Zhang, L. Texture weakening of AZ31 magnesium alloy sheet obtained by a combination of bidirectional cyclic bending at low temperature and static recrystallization. *J. Mater. Sci.* **2013**, *48*, 913–919. [[CrossRef](#)]

23. Yan, H.; Chen, R.S.; Han, E.H. Room-temperature ductility and anisotropy of two rolled Mg–Zn–Gd alloys. *Mater. Sci. Eng. A* **2010**, *527*, 3317–3322. [[CrossRef](#)]
24. Xin, Y.; Wang, M.; Zeng, Z.; Huang, G.; Liu, Q. Tailoring the texture of magnesium alloy by twinning deformation to improve the rolling capability. *Scripta Mater.* **2011**, *64*, 986–989. [[CrossRef](#)]
25. He, J.J.; Mao, Y.; Fu, Y.J.; Jiang, B.; Xiong, K.; Zhang, S.; Pan, F. Improving the room-temperature formability of Mg–3Al–1Zn alloy sheet by introducing an orthogonal four-peak texture. *J. Alloys Compd.* **2019**, *797*, 443–455. [[CrossRef](#)]
26. Steiner, M.A.; Bhattacharyya, J.J.; Agnew, S.R. The origin and enhancement of {0001}<11-20> texture during heat treatment of rolled AZ31B magnesium alloys. *Acta Mater.* **2015**, *95*, 443–455. [[CrossRef](#)]
27. Huang, X.S.; Suzuki, K.; Chino, Y. Influences of initial texture on microstructure and stretch formability of Mg–3Al–1Zn alloy sheet obtained by a combination of high temperature and subsequent warm rolling. *Scripta Mater.* **2010**, *63*, 395–398. [[CrossRef](#)]
28. Jiang, M.G.; Yan, H.; Chen, R.S. Enhanced mechanical properties due to grain refinement and texture modification in an AZ61 Mg alloy processed by small strain impact forging. *Mater. Sci. Eng. A* **2015**, *621*, 204–211. [[CrossRef](#)]
29. Jiang, M.G.; Yan, H.; Chen, R.S. Twinning, recrystallization and texture development during multi-directional impact forging in an AZ61 Mg alloy. *J. Alloys Compd.* **2015**, *650*, 399–409. [[CrossRef](#)]
30. Zhu, S.Q.; Yan, H.G.; Liao, X.Z.; Moody, S.J.; Sha, G.; Wu, Y.Z.; Ringer, S.P. Mechanisms for enhanced plasticity in magnesium alloys. *Acta Mater.* **2015**, *82*, 344–355. [[CrossRef](#)]
31. Sanjari, M.; Kabir, A.S.H.; Farzadfar, A.; Utsunomiya, H.; Petrov, R.; Kestens, L.; Yue, S. Promotion of texture weakening in magnesium by alloying and thermomechanical processing. II: Rolling speed. *J. Mater. Sci.* **2014**, *49*, 1426–1436. [[CrossRef](#)]
32. Huang, X.S.; Chino, Y.; Mabuchi, M.; Matsuda, M. Influences of grain size on mechanical properties and cold formability of Mg–3Al–1Zn alloy sheets with similar weak initial textures. *Mater. Sci. Eng. A* **2014**, *611*, 152–161. [[CrossRef](#)]
33. Song, B.; Xin, R.L.; Liao, A.L.; Yu, W.B.; Liu, Q. Enhancing stretch formability of rolled Mg sheets by pre-inducing contraction twins and recrystallization annealing. *Mater. Sci. Eng. A* **2015**, *627*, 369–373. [[CrossRef](#)]
34. Zhang, H.; Huang, G.S.; Wang, L.F.; Jørgen Roven, H.; Xu, Z.; Pan, F. Improved ductility of magnesium alloys by a simple shear process followed by annealing. *Scripta Mater.* **2013**, *69*, 49–52. [[CrossRef](#)]



© 2020 by the authors. Licensee MDPI, Basel, Switzerland. This article is an open access article distributed under the terms and conditions of the Creative Commons Attribution (CC BY) license (<http://creativecommons.org/licenses/by/4.0/>).